A BIO-INSPIRED OPTIMIZER BASED ANN CONTROLLER FOR EV CHARGING STATION WITH GRID TIED PV SYSTEM

Dr Balaji V[1], Dr Nethravathi P. S.[2]
[1] *Post – Doctoral Research Scholar , Dept of Computer Science Engineering, Institute of Engineering and Technology, Srinivas University, Mangalore -575001,India,E-Mail:balajieee79@gmail.com*
[2] *Professor, College of Computer Science & Information Science, Srinivas University, Mangalore-575001,India,E-mail:nethrakumar590@gmail.com*

ABSTRACT

Nowadays, scientists have more interest towards the challenge of establishing an extremely effective emission-free energy generating and transportation infrastructure to tackle serious demand for ecological disaster driven on by greenhouse gas emissions and global warming. The Electric Vehicles (EVs) are developed to tackle the problem of emission-free mobility, whereas Photovoltaic (PV) systems are deployed and expanded to address the need for carbon free power generation. The use of PV-powered electric vehicles further reduces the amount of carbon dioxide emitted into the atmosphere. Hence, in this work concentrates on towards hybrid PV system and grid with EV, that is strongly emit the harmful gases from atmosphere with less distortion. By the utilization of Integrated High Gain Boost-Cuk (IHGBC) Converter, the poor level of output voltage is stabilized and also it provides minimized switching loss. Here, Artificial Neural Network (ANN) based DC link voltage approach is used to control the IHGBC converter. The Salp Swarm Optimized algorithm is intended for tuning the hyper-parameters of ANN (SS-ANN). The regulation of single-phase Voltage Source Inverter (1ϕ VSI) linked to the grid is accomplished deploying a Proportional Integral (PI) controller. To verify the performance of suggested ANN, the MATLAB platform is implemented. The simulation findings demonstrate that ANN-based control technique outperforms other control approaches. The suggested converter obtains excellent efficiency of 94% with reduced THD value of 2.12%, making it suitable for usage in PV-based EV applications.

Keyword : - *PV, EV, IHGBC converters, SS-ANN, PI controller.*

1. INTRODUCTION

Currently, EVs are replacing conventional internal combustion engine (ICE). But in reality, ICEs have a variety of shortcomings that EVs potentially help to overcome. Compared to ICEs, EVs produce very less pollutants, are more energy efficient, make less noise, and require less maintenance [1, 2]. The construction of the charging stations, the period of the charging process, and the impact of these stations on the current electrical grid are just a handful of challenges which indeed to be overcome. By using quick charging methods, the charging period is drastically decreased to only a few minutes. Such methods impose large load demand and harmful impacts on the electricity grid [3, 4]. Specifically when a significant amount of filling stations are linked to the electrical grid instantaneously, numerous issues arise, including extreme overloading, unstable power, and voltage change [5-7]. The improvement of the electrical system is one resolution for such issues, but it is expensive. Using an Energy Storage System (ESS) that serve as a barrier between the utility and the EV Charging Station (EVCS) is also a superior approach [8]. The utility grid will sense less strain with the deployment of ESS, but this is still a challenge due to the anticipated high number of EVCSs in the upcoming years.

Thus, it is necessary to use clean energy sources in EVCS to highlight the effects of EV on the atmosphere. Renewable Energy Sources (RES) are generally intermittent instead of constant. Photovoltaic (PV), wind systems and bioenergy are the most frequently employed RES for EV charging systems [9, 10]. Compared to wind energy

systems, PV energy systems are easier to operate as well as more efficient. Deployment of EVs powered by solar energy is essential for tackling environmental issues in an efficient manner. Since the PV module's voltage output is so poor, a suitable DC-DC converter needs to be employed to produce enhanced voltage level. Due to its realistic structure and flexibility for voltage enhancing functions, the Boost converter [11] is one of the commonly utilized converters for PV systems. The substantial losses and voltage regulation across the switches make it less than optimal for applications demanding step-down voltage conversion. Using a Buck-Boost converter [12-15] enables the conversion of voltage in both step-up and step-down modes, but on the downside, the outcome has inverted polarity and the input current is interrupted. The Cuk converter has continuous input current [16] but, like the Buck-Boost converter, it also has reversed output polarity. In order to overcome these issues the IBC converter with coupled inductor is proposed here, which is more efficient with reduced switching losses.

To provide the finest optimum solutions, various Meta-heuristic algorithm optimisation methods and control approaches are mostly presented out. A number of methods, including Grey Wolf Optimization (GWO) [17], Particle Swarm Algorithm (PSO) [18], Genetic Algorithmic Technique (GA) [19], and Whale Optimization Algorithm (WOA) [20], have been investigated to enhance the effective solution. Nevertheless, these methods offer low solution accuracy and slow convergence speed. In comparison to existing metaheuristic algorithms, the Salp Swarm Optimization method (SSO) has recently been revealed to offer a better solution in handling a number of challenging engineering problems [21]. The ANN based control method is used to enhance the performance of IHGBC converter together with SSO algorithm for tuning the hyper parameters of ANN in effective manner [22]. The PI controller is being utilized extensively in various fields. The basic requirement for employing this controller is to adjust their parameters to achieve the desired outcome. So, it is essential to implement a technique that is simple to use, extremely accurate, and quick to determine the control parameters (K_p , K_i). This is suitable because of its uncomplicated design, which is simple to comprehend and accomplish [23-25]. The application of a suitable PI controller is considered to be essential to improve the converter's dynamic qualities for generating a reliable and regulated output. Because of its simplistic and effective design, a PI controller serves primarily to regulate the functionality of the converters in a PV system. The contribution of this work involves grid incorporated PV based EV to reduce the harmful gas from atmosphere and conceivable power production [26-27]. By the implementation of IHGBC converter, the poor output voltage of PV is enhanced. With the assistance of ANN control approach the performance of IHGBC converter is improved. The operation of single phase VSI which is linked to the single phase grid is controlled by a PI controller.

2. PROPOSED SYSTEM DESCRIPTION

In this paper, a grid connected PV based EVCS is suggested as an approach to enable mobility and defensible decarbonized energy production. In addition to promoting and simplifying the adoption of EVs in rural areas, the proposed PV-based EVCS is aimed at decreasing the heavy reliance on the grid for power supply in metropolitan areas. The Fig 1 illustrates the schematic diagram for grid incorporated PV based EV system. An IHGBC converter specifically developed for the PV system with the goal of increasing output voltage, significantly reduce steady state error and stabilise converter output. The optimized ANN controller helps to enhance the performance of proposed converter. With the assistance of the optimised ANN controller, the converter's output fluctuations are regulated and a constant output is obtained. A single phase VSI receives the converter's strengthened output and deploys it to produce an inverted output with lower THD.

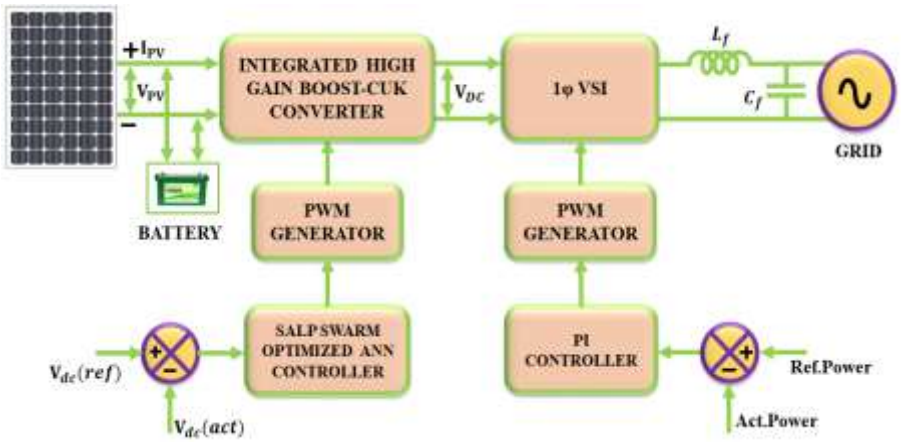

Fig -1: Schematic representation of proposed system

3. PROPOSED SYSTEM MODELLING

3.1 PV System Modelling

Several PV cells are combined in parallel and series in a PV module to achieve the required level of current or voltage. The PV cell is essentially a large-area p-n junction semiconductor diode. A basic PV cell equivalent circuit based on the single diode approach is shown in Fig 2.

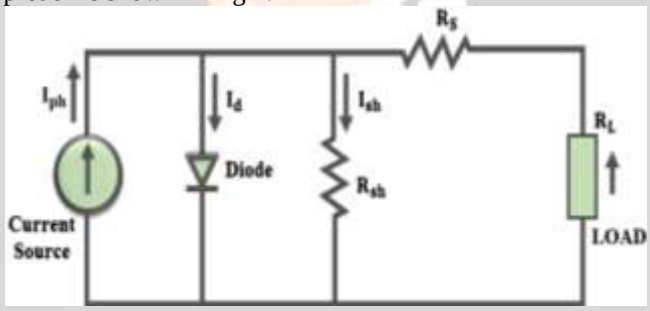

Fig -2: PV equivalent circuit

The PV cell output equation is written as,

$$I_c = I_{ph} - I_0 = I_{ph} - I_{sat}\left[e^{\frac{q}{AKT_c}(V+IR_S)} - 1\right] \quad (1)$$

Where, the Boltzmann constant, Temperature cell, stack internal resistance and identity factor are represented by *K*, T_c, R_s *and A* respectively. PN junction reverse saturation current, photocurrent, and electron charge are referred to by these terms I_{sat}, I_{ph} *and q*. A PV system is able to produce the required energy by considering the combinations of panels in series and parallel. The outcome from the PV panel is significantly increased by employing an appropriate converter and in this paper, an integrated IBC converter with coupled inductor is used.

3.2 IHGBC Converter Modeling

The proposed IHGBC comprises the configuration of High Gain Boost converter and Conventional Cuk converter. The Figure 3 illustrates the circuit diagram for IHGBC converter, which enhances the voltage gain by accompanying the benefits of both high gain boost and classical Cuk converters. With the aid of a single power switch, the IHGBC converter operates in continuous current mode, bringing minimized voltage stress on regulated switch and diodes.

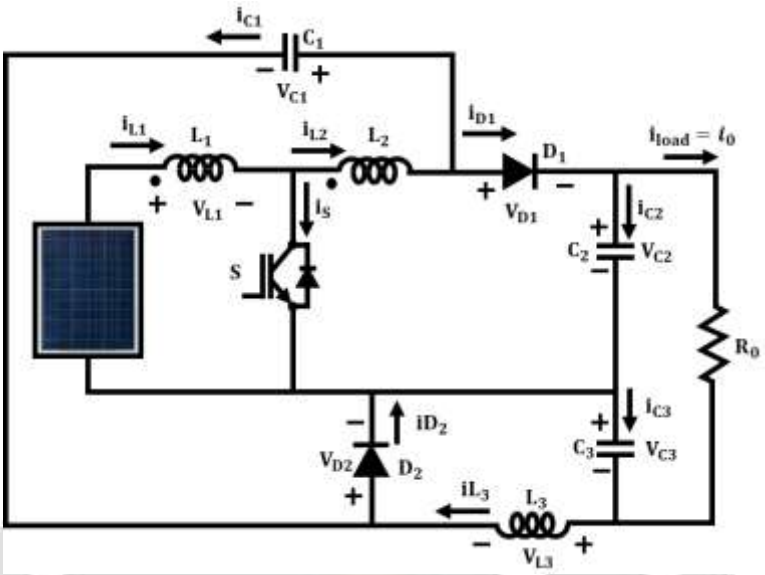

Fig -2: Equivalent Configuration of IHGBC Converter

The following is taken into consideration when analysing the proposed scheme DC-DC converter mode operations, capacitors (C1, C_2, C3) and inductors (L_1, L_2, L_3) charging and discharging.

Phase 1: $[t_1 - t_2]$

At instance when $t = t_1$, the switch (S) is ON, and the inductors (L_1, L_2 and L_3) charges and capacitor C_1 discharges via S. At the same time the inductor L_3 and the diodes (D_1 and D_2) are limiting with respect to V_{C1} and V_{C2} respectively

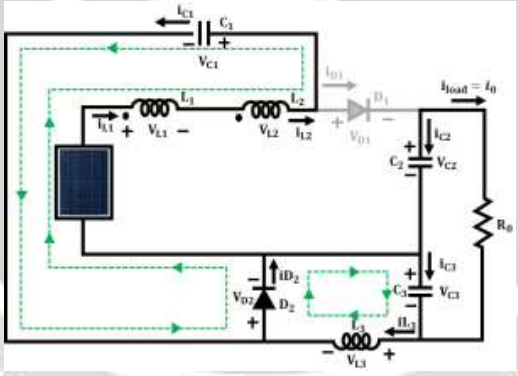

Fig -3: **(a)** Phase 1

Phase 2: $[t_1 - t_2]$

In this mode switch is set to OFF position. Currently, the voltage of capacitor V_{C2} is greater than V_{C1}. As a result, C_1 is charged and the inductors L_1, $L_2$$and$ $L_3$are discharged after the specified interval of time t_2. And the diode D_1 is still under reverse bias at this time, diode D_2 is conducts continuously**.** Henceforth, the voltage stress across diodes is equal to voltage across switch.

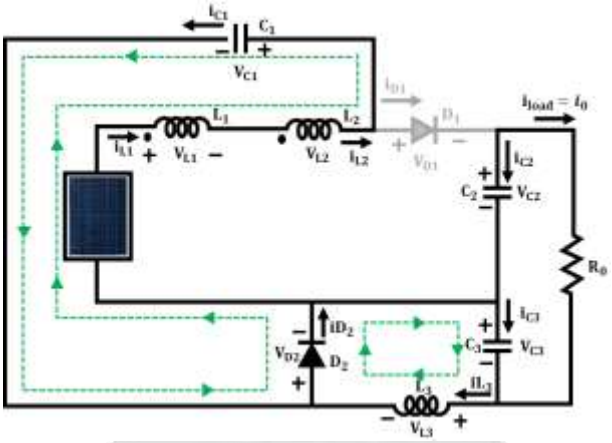

Fig -3: **(b)** Phase 2

In general, the choice of input inductor for converter is made based on converter's conduction mode, amount of load current required, and desire to ensure least amount of output current ripple. As a result, input inductor L_1 *and* L_2 value is selected to have a low current ripple Δ_{iL}. On applying Kirchhoff's law to phase 1, the capacitor values are expressed as

$$-V_{pv} + V_{L1} + V_{L2} = 0 \Rightarrow V_{L1} + V_{L2} = V_{pv} \quad (2)$$

$$-V_{C1} + V_{L3} + V_{C3} = 0 \Rightarrow V_{L3} = -V_{C3} + V_{C1} \quad (3)$$

$$i_S + i_{L1} - i_{L2} - i_{C1} = 0 \quad (4)$$

$$i_O - i_{L3} - i_{C3} = 0 \quad (5)$$

$$i_{C1} = -i_{L1} - i_{L2} \quad (6)$$

$$i_{C2} = -i_O \quad (7)$$

At Phase 2, switch S in OFF state, and the capacitor C_2 and C_3 attains energy from the coil, and it is verified using loops.

$$-V_{pv} + V_{L1} + V_{L2} + V_{C1} = 0 \quad (8)$$

$$V_{L1} + V_{L2} = -V_{C1} + V_{pv} \quad (9)$$

$$V_{L3} + V_{C3} = 0 \Rightarrow V_{L3} = -V_{C3} \quad (10)$$

$$V_{C1} = V_{C2} \quad (11)$$

From Figure 3(b) the capacitor current i_{C1} *and* i_{C2} is expressed as,

$$i_{C1} = (i_{L1} + i_{L2}) - i_{D1} = i_{D2} - i_{L3} \quad (12)$$

$$i_{C2} = i_{D1} - i_O \quad (13)$$

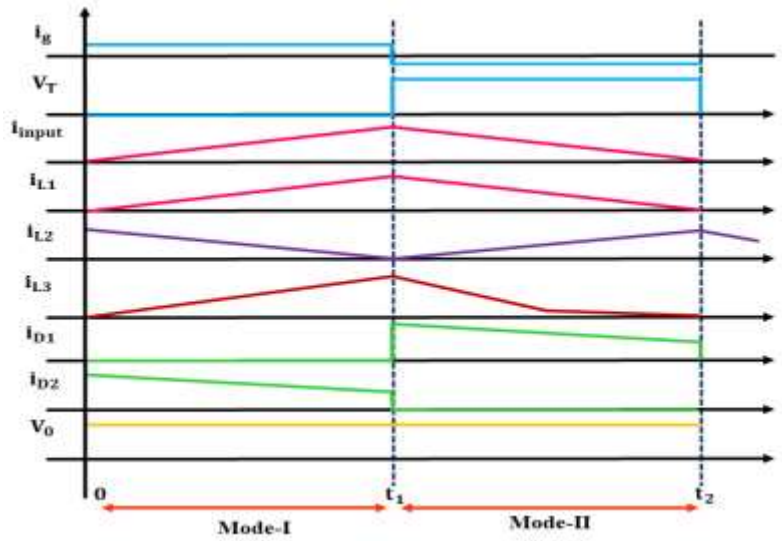

Fig -4: Waveform for modes of operation

Fig 4 waveform represents the continuous conduction mode operation of IHGBC converter. The operation of converter is enhanced with help optimized ANN controller, which is explained briefly forthcoming section.

3.3 SALP SWARM Optimized ANN Controller

3.3 .1 ANN Control Strategy

Normally, an ANN is a system including one or more hidden and neurons within every layer. As an outcome, the behaviour of an ANN is exactly equivalent with the response of a realistic neural network. The feed-forward ANN, also known as the FF-ANN, is utilised in this work. The input in FF-ANN simply progresses in the forward direction. Mathematically, a particular neuron's action is described as:

$$y = Act\ (b + \sum_{i=1}^{M} x_i w_i)\ , \tag{14}$$

Where, the activation functions are represented by $Act(.)$,w_i, b and M, correction and bias factor, x_i is every input weights, and amount of input components correspondingly, where the input characteristics $x = \{x_1, x_2, \dots x_m\}$. An FF-ANN layer might be constructed by combining the several neurons together into single layer. The following is able to symbolize the overall solution employed to determine the outcome of single-output multi-input FF-ANN:

$$\begin{aligned} y_1 &= Act\left(\sum_{j=1}^{J} {}_2w_{j1} h_j + {}_2b_1\right), and \\ h_j &= Act\left(\sum_{m=1}^{M} {}_1w_{mj} x_m + {}_1b_j\right), \forall j = \{1, \dots, J\}, \end{aligned} \tag{15}$$

When $y_1$is the outcome of the ANN, ($_1w_{mj}$,$_2w_{j1}$) denotes the hidden and output layers' weights, J denotes the hidden layers' number, M denotes the input neurons' number, and ($_1b_j$, $_2b_1$) denotes the layers' corresponding biases.

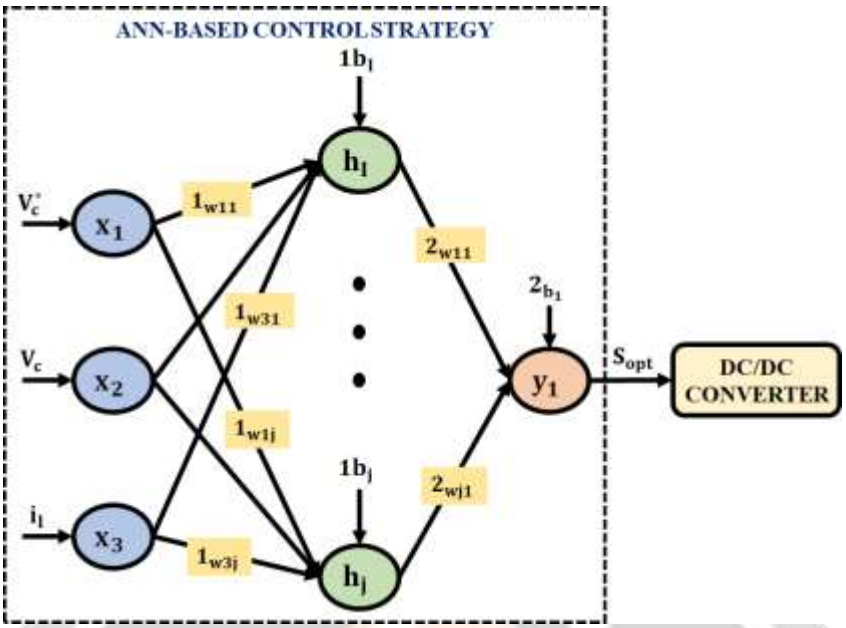

Fig -5: Proposed ANN control approach

The Fig 5 illustrates the schematic representation of suggested ANN based DC link control. In this paper, the optimum switching state S_{Opt} is taken into consideration as controlling method's output, whereas reference dc voltage as ($V_{dc\ ref}$), actual dc voltage as ($V_{dc\ act}$), and inductor current as i_l are selected as input characteristics of developed ANN-based control method. The 15-neuron design is selected using hyper parameters tuning approach. The ANN is trained, and biases and weights are modified, through using Bayesian Regularised Approach (BRT). BRT helps to lessen or completely replace the requirement for time-consuming cross validation because it is more reliable than conventional propagation techniques.

Fig -6: Confusion ANN's training matrix

In this article, the ANN is trained using 60% of the randomized input data, 20% for testing, and 20% for verification. The total confusion matrix, shown in Fig 6, is utilised to evaluate the trained ANN's accuracy. The diagonal matrix components that show the accurate categorization of the data class, whereas other elements display the incorrect classification of the data.

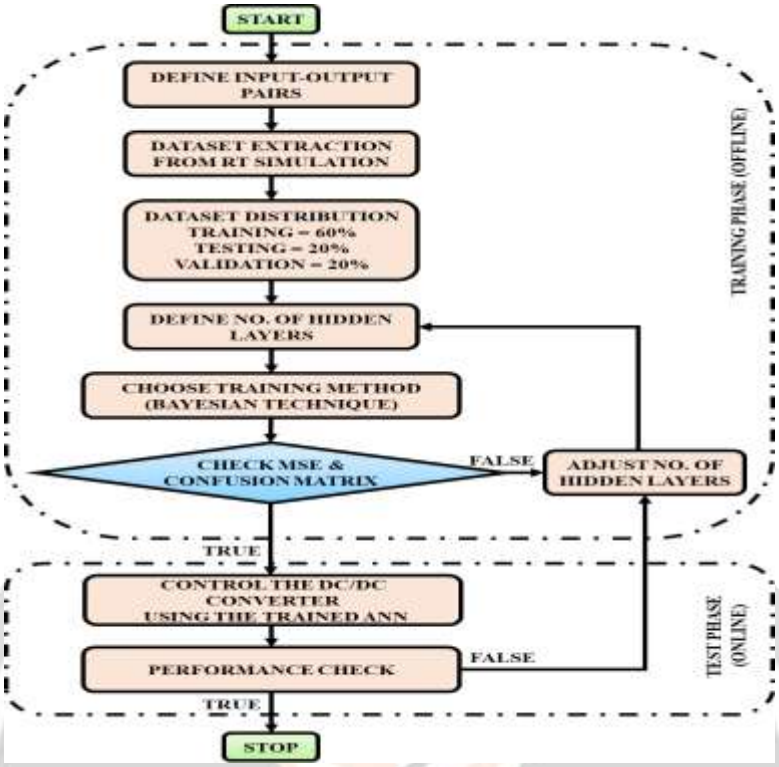

Fig -7: Main tasks in implementing IHGBC Converter with ANN-based control method

To estimate trained ANN performance of model under the situations, it is transferred to simulink. In conclusion, Fig 7 depicts the entire process of the learning-based control method, emphasizing the important phases of the test and training phases. In order to adjust the control hyper parameters of ANN controller, the SSO algorithm is implemented. The detailed description of SSO algorithm is explained as follows.

3.3 .2 SSO Algorithm

Seyedali Mirjalili developed the SSO algorithm, which is employed in a variety of sectors. For instance, the SSA-based methodology appears to be capable of identifying an ideal segmentation results that increases classification performance while minimizing the amount of picked input characteristics, according to the outcomes. Moreover, it's possible to employ it to modify the hyper-parameters of machine learning models such as neural networks. The salp, an aquatic organism, and its predation behaviour served as the basis for the central concept of salp. The salps frequently create a swarm known as a salp chain and proceed to the food production that has yet to be properly explained. The population of SSA is split into two categories: Depending on their position within the network, there are leaders and followers. The chain's leader is in the front, and its members follow it. Assume that n variables must be estimated for the above model, where x represents the location of a salp and y represents the food source, which designates the swarm's intended destination in the search space. Salp updates the leader's position by (16)

$$x_i^1 = \begin{cases} y_i + r_1\left((ub_i - lb_i)r_2 + lb_i\right) & r_3 \geq 0 \\ y_i - r_1\left((ub_i - lb_i)r_2 + lb_i\right) & r_3 < 0 \end{cases} \quad (16)$$

Where y_i is the location of the food in the ith dimension and x_i^1 is position of the first salp in ith dimension. The ith dimension lower bound and upper bound are represented by lb_i and ub_i, respectively and the three random numbers are r_1,r_2 and r_3.

Since it combines exploitation and exploration during the whole search process, r_1 has a prominent position among the three random integers. It is described as

$$r_1 = 2e^{-\left(\frac{4l}{L}\right)^2} \tag{17}$$

Where l denotes present iteration, L denotes maximum number of iterations, and r_2 r_3 denote random values between $[0, 1]$. According to Newton's law of motion, the' positions are updated using the following equation:

$$x_i^j = \frac{1}{2}\lambda t^2 + \delta_0 t \tag{18}$$

Where $j \geq 2, x_i^j$ location of jth salp in ith dimension, t is time, δ_0 is initial speed and $\lambda = \delta_{\frac{final}{\delta_0}}$, $Where\ \delta = \frac{x - x_0}{t}$. The previous formula can be changed into the following form by assuming that $\delta_0 = 0$ and t equals the number of iterations in an optimal control problem.

$$x_i^j = \frac{1}{2}\left(x_i^j + x_i^{j-1}\right) \tag{19}$$

Where $j \geq 2$. this equation demonstrates how the subsequent salps update their position based on their own and the previous salp's positions.

The limiting equation will force certain salps to return to the boundaries if they venture outside the restricted search area:

$$x_i^j = \begin{cases} l^j & if\ x_i^j \leq l^j \\ u^j & if\ x_i^j \geq u^j \\ x_i^j & otherwise \end{cases} \tag{20}$$

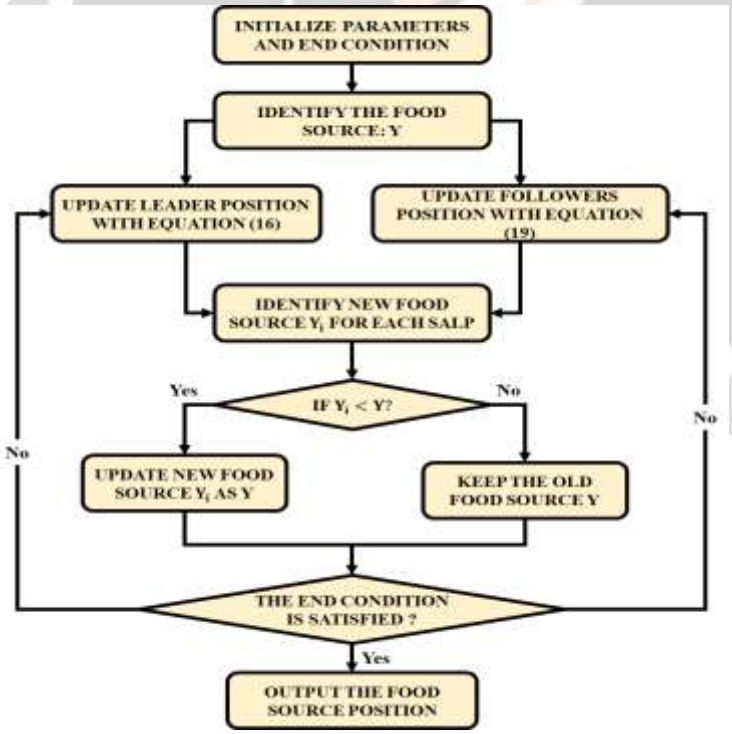

Fig -8: Flowchart representation of SSA

Algorithm 1 The procedure of Salp Swarm (SSA) Algorithm

Require: *Initialize the salp population* x_i $(i = 1, 2 \dots n)$ *consider ub and lb.*

while *(End condition is not satisfied)*

Calculate the fitness of each search salp

F = *the best search solution*

Update r_1 *by Equation*(4)

for *each salp* (x_i)

if $(i == 1)$

Update the position of the leading salp by Equation(3)

else

Update the position of the followers salp by Equation(6)

end

end

Verify the position of salps based on the upper and lower bounds

end

return F

Even till the end condition is satisfied, all of the changes mentioned above are carried out iteratively. It ought to be noted that the food source may occasionally change as a result of the salp chain's ability to explore and utilise the area surrounding an existing solution to discover a better one. For other terms, throughout optimisation, the salp chain has the capacity to move in the direction of the global optimal solution. The SSA's method is demonstrated in Algorithm 1, which demonstrates where it begins by beginning numerous salps with random positions, iteratively updates these positions, and then finally finds a global optimisation solution. Figure 8 depicts the SSA's flowchart. The hyper parameter of the ANN controller is fine-tuned with the aid of SSA, and it also effectively ensures the constant voltage across the DC link.

3.3 .3 PI Controller

The most suitable controllers in various sectors is the PI controller. The fundamental requirement in using these controllers is to adjust their parameters to achieve the desirable outcome. So, it is necessary to employ a technique that is simple to use, highly accurate, and quick to determine these control parameters (K_p, K_i). Fig 9 illustrates the system model for the PI controller.

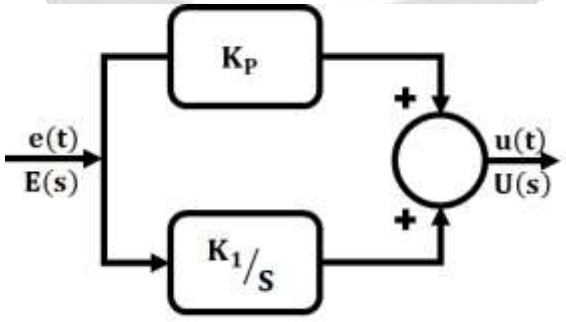

Fig -9: Schematic Diagram of PI controller

Equation (21), in which K_p is the proportional gain and K_i is the integral gain states the general equation of the PI controller**.**

$$u(t) = k_p e(t) + k_i \int e(t)\,dt \tag{21}$$

Equation (10) is modified to Equation (11) using the Laplace transform

$$U(s) = k_p E(s) + \frac{k_i E(s)}{s} \tag{22}$$

Equation is the expression of PI with respect to the duration constraints (22)

$$U(s) = k_p[1 + \frac{1}{\tau_i}]E(s) \tag{23}$$

Where $k_i = \frac{k_P}{\tau_i}$ *and* $k_p = k_d/\tau_i$

The proportional and integral terms give the error signal more stable operation and lower the model's steady-state error. When K_p and K_i values are properly tuned for a closed-loop control system, the rise time is slightly reduced and the settling time is improved. To help with controller tuning, several software-based concepts have been implemented. The proposed PI controller successfully enhance the performance of single phase VSI.

3.3 .4 Modelling of Single Phase VSI

The constant DC link voltage is converted into AC with help of single phase VSI topology is illustrated in Fig 10.

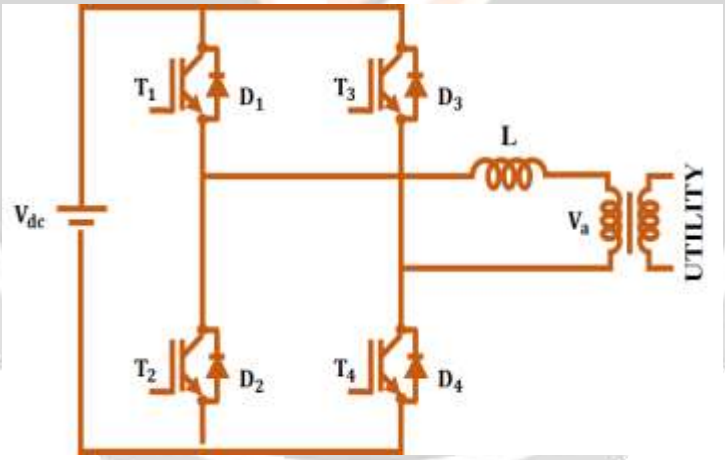

Fig -10: Single Phase VSI

It is comprised of a dc voltage source; four power switches T_1,T_2, T_3 and T_4 , four diodes D_1, D_2, D_3, and D_4. The inverter output is linked to the grid via LC filter which minimize the harmonics and maintain the sinusoidal waveform.

4. RESULTS AND DISCUSSION

An efficient hybrid optimization algorithm for PV based EV charging station using IHGBC converter is discussed in this research. In this section, the suggested control approach is verified using MATLAB platform, and the attained outcomes are presented below. Table 1 represents the parameter specification of proposed method.

Table -1: Parameter Specifications

Parameter	Specification
Solar PV System	
Series connected solar PV cells	36
Open Circuit Voltage	$12V$
Short Circuit Current	$8.33A$
Peak Power	$10KW$, 10 Panels
Integrated High Gain Boost-Cuk	
$L_1,\ L_2, L_3$	$1mH$
C_1, C_2	$2200\mu F$
C_3	470 μF

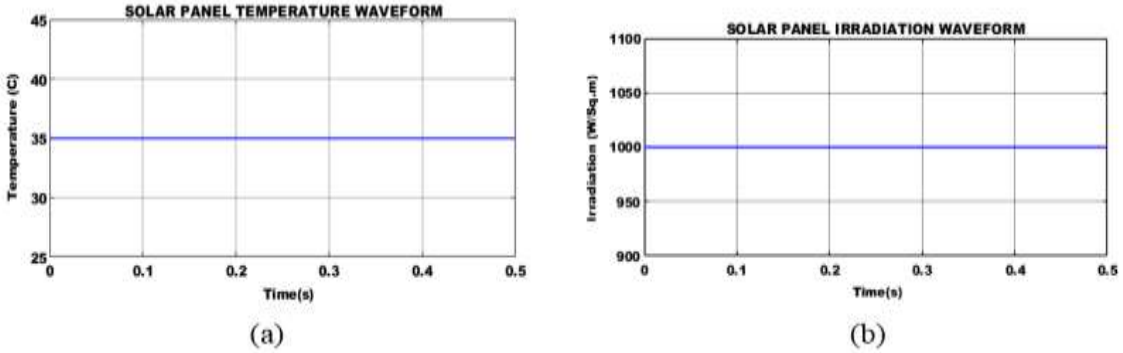

Fig -11: Waveforms illustration of solar panel (a) Temperature and (b) Irradiation

A PV system functioning on renewable energy is connected to the converter in order to evaluate the integrated Boost-Cuk converter's effectiveness. The temperature remained stable at 35°C as can be seen from the waveform observation in Fig 11(a), and this information can be employed to estimate the level of proposed method which is tackles the intermittent nature of the PV system. According to this, Figure 11 (b) shows a PV system that achieves irradiation of 1000 W/Sq.m.

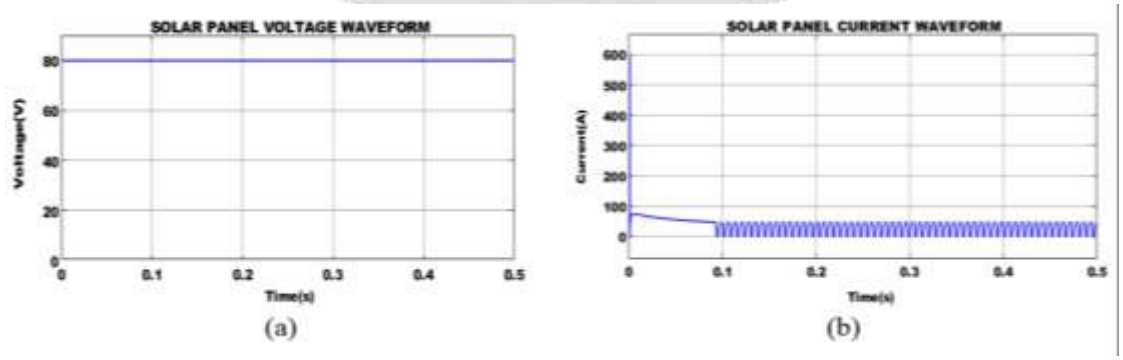

Fig -11: Waveforms illustration of solar panel (a) Voltage and (b) Current

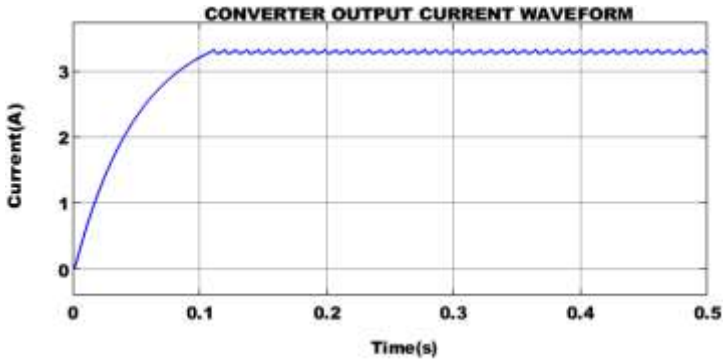

Fig -13: Waveforms illustration of converter output current

The proposed converter output current waveform is demonstrated in Fig 13. After 0.13 sec, the output current maintains constant value of 3.5A.

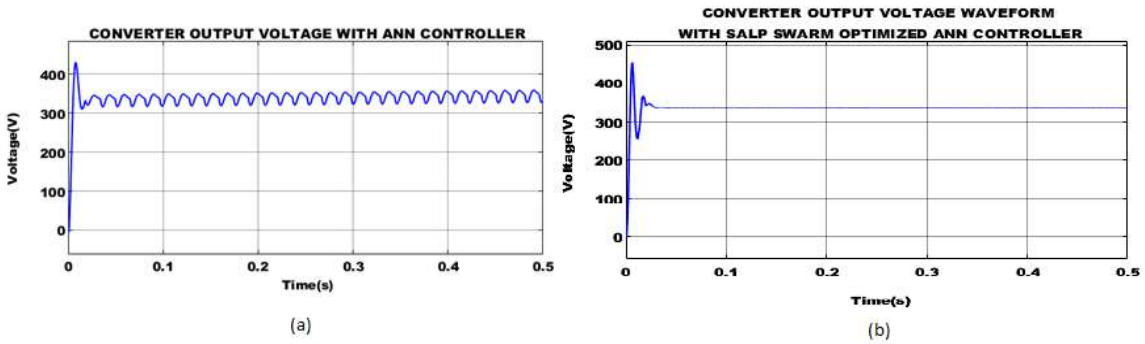

Fig -14: Waveforms illustration of (a) output voltage of ANN controller (b) output voltage of SS- ANN controller

Fig 14 demonstrates the converter output utilizing SS optimized ANN controller. From the waveform it is clear that the constant voltage of 330V is maintained at 0.05sec depicted in Figure 14 (a) and similarly, the SS optimized ANN controller maintains stable voltage of 340V at 0.05 sec as illustrated in Figure 14 (b).

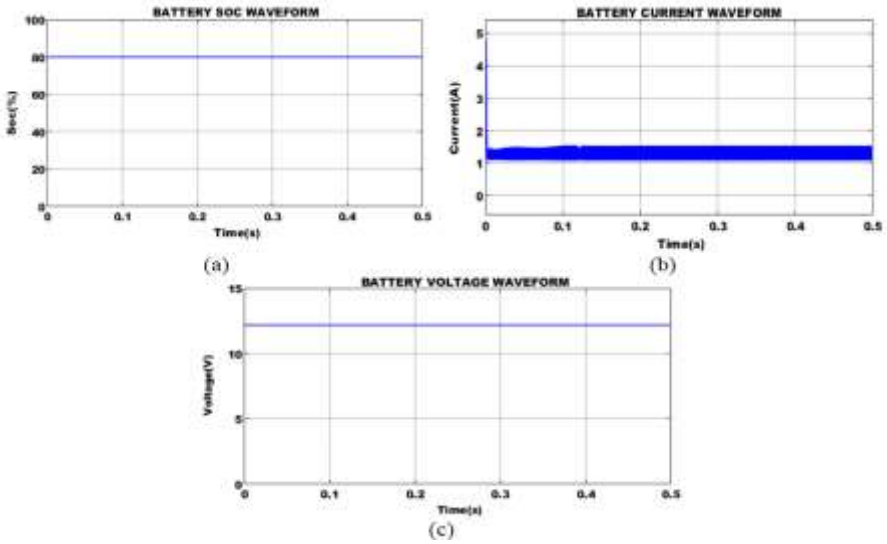

Fig -15: Waveforms illustration of Battery (a) SOC (b) Voltage (c) Current

The waveforms for batteries are shown in Fig 15. Figure 15(a) demonstrates that the battery's SOC is maintained at 80%. Figure 15(b) indicates that the current value of 1.3A is maintained. Similarly, the Figure 15(c) denotes the stable voltage of 12V is maintained.

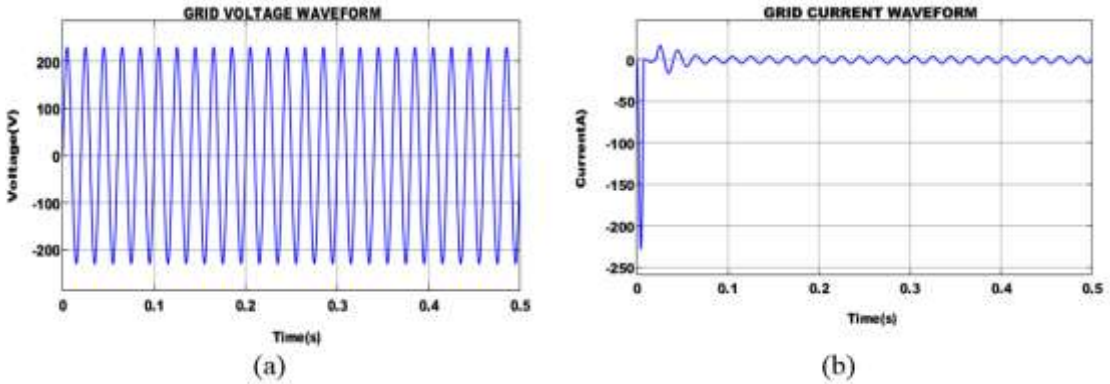

Fig -16: Waveforms illustration of Grid (a) Voltage (b) Current

The voltage and current waveforms of 1 ϕ grid is shown in Fig 16.The constant grid voltage of 220V is depicted in Fig 16(a), similarly the current waveform of grid becomes constant after 0.06 sec at 4A magnitude as shown in fig 16(b).

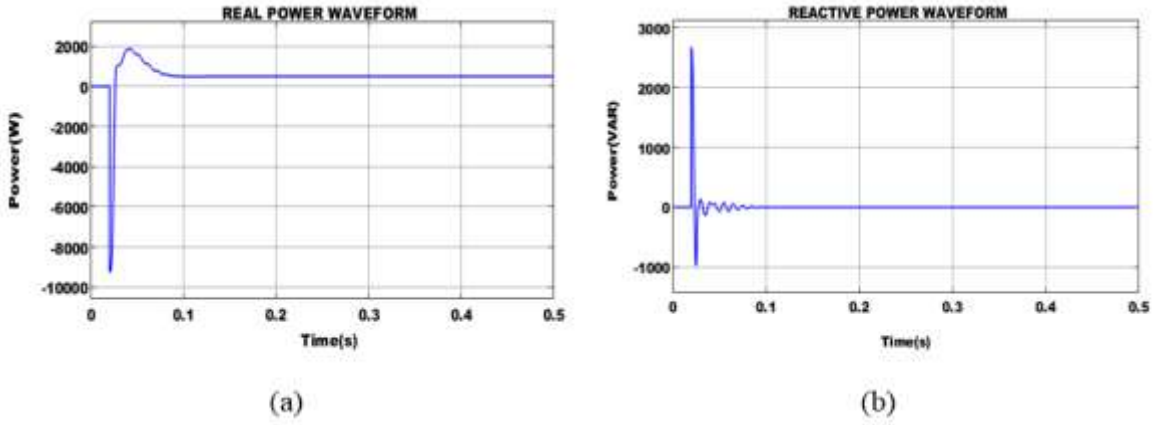

Fig -17: Waveforms illustration of (a) Real Power (b) Reactive Power

Fig17 shows the waveforms that indicate the reactive and real power of the 1 ϕ grid. Real power achieves a fixed value of 830W at 0.1 seconds and zero reactive power is obtained

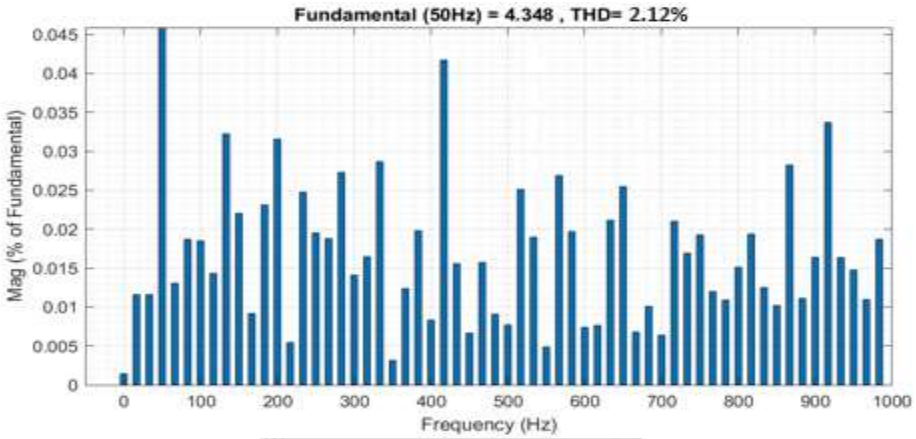

Fig -18: THD value

The intended converter THD value of 2.12% with reduced harmonics is displayed in Fig18.

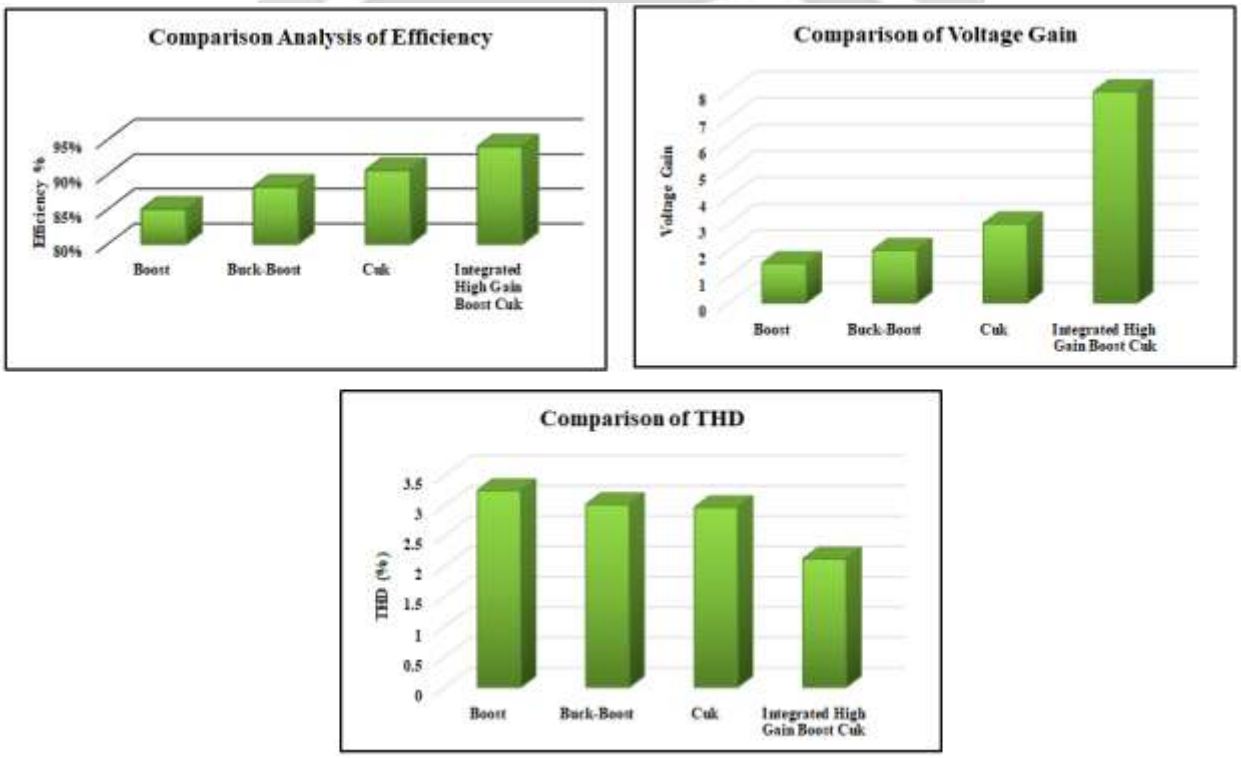

Fig -18: Comparison analysis of IHGBC converter with different converters

Fig 18 indicates the comparison analysis of IHGBC converter with various converters. From the graph observation, is it noted that, the suggested IHGBC converter generates an efficiency of 94% and voltage gain 1:8 with minimized THD value of 2.12%.The obtained outcomes show that the presented method is highly effective in contrast to other techniques.

4. CONCLUSION

To promote the deployment of electric vehicles as primary mode of transportation in the future, a reliable grid incorporated PV based EVCS has been designed. A PV-based EVCS is suggested in this paper with the intention of reducing carbon emissions and the objective of extending the reach of EVs even in the most underdeveloped regions. The low output voltage level is regulated through the use of IHGBC Converter, which also offers minimal power losses. Thus, the IHGBC converter is controlled using a DC link voltage control method that is based on ANN controller. With the help of SSO algorithm, ANN controller hyper parameters are tuned optimally. A PI controller is used to regulate the performance of 1 ϕ VSI linked to the grid. The simulation outcomes demonstrate that under a range of loading circumstances, ANN-based control approach performs better. From the attained results, it is clear that the suggested method has high efficiency of 94% and lowest THD value of 2.12% with negligible harmonics.

6. REFERENCES

[1].Kavin, K. S., and P. Subha Karuvelam. "PV-based grid interactive PMBLDC electric vehicle with high gain interleaved DC-DC SEPIC Converter." *IETE Journal of Research (2021*), pp.1-15.

[2]. Atawi, Ibrahem E., Essam Hendawi, and Sherif A. Zaid. "Analysis and design of a standalone electric vehicle charging station supplied by photovoltaic energy." *Processes* 9.7 (2021): 1246.

[3].Singh, Bhim, et al. "Implementation of solar PV-battery and diesel generator based electric vehicle charging station." *IEEE Transactions on Industry Applications* 56.4 (2020): 4007-4016.

[4]. Dai, Qiongjie, Jicheng Liu, and Qiushuang Wei. "Optimal photovoltaic/battery energy storage/electric vehicle charging station design based on multi-agent particle swarm optimization algorithm." *Sustainability* 11.7 (2019): 1973.

[5].Zhang, Yongmin, Pengcheng You, and Lin Cai. "Optimal charging scheduling by pricing for EV charging station with dual charging modes." *IEEE Transactions on Intelligent Transportation Systems* 20.9 (2018): 3386-3396.

[6].Mateen, Suwaiba, et al. "Discrete Stochastic Control for Energy Management With Photovoltaic Electric Vehicle Charging Station." *CPSS Transactions on Power Electronics and Applications* 7.2 (2022): 216-225.

[7]. Fachrizal, Reza, et al. "Optimal PV-EV sizing at solar powered workplace charging stations with smart charging schemes considering self-consumption and self-sufficiency balance." *Applied Energy* 307 (2022): 118139.

[8]. Minh, Phap Vu, Sang Le Quang, and Manh-Hai Pham. "Technical economic analysis of photovoltaic-powered electric vehicle charging stations under different solar irradiation conditions in Vietnam." *Sustainability* 13.6 (2021): 3528.

[9]. Jiang, Wei, and Yongqi Zhen. "A real-time EV charging scheduling for parking lots with PV system and energy store system." *IEEE Access* 7 (2019): 86184-86193.

[10]. Hassoune, A., et al. "Power management strategies of electric vehicle charging station based grid tied PV-battery system." *International Journal of Renewable Energy Research* 8.2 (2018): 851-860.

[11]. Mohamed, Ahmed AS, et al. "Grid integration of a PV system supporting an EV charging station using Salp Swarm Optimization." *Solar Energy* 205 (2020): 170-182.

[12]. Nayak, P. Srinivasa Rao, et al. "Design and Simulation Of BUCK-BOOST Type Dual Input DC-DC Converter for Battery Charging Application in Electric Vehicle." *2021 International Conference on Sustainable Energy and Future Electric Transportation (SEFET)*. IEEE, 2021.

[13]. Pradhap, R., et al. "Solar Powered Hybrid Charging Station For Electrical Vehicle." *Int. J. Eng. Technol. Res. Manag* 4 (2020): 19-27.

[14]. Krithiga, S., et al. "FLC-based, PV-fed interleaved dual buck-boost converter for EV battery charging applications." *Heliyon* 8.4 (2022): e09238.

[15].Thomas, Sarah Mary, and S. Sheik Mohammed. "Solar powered EV charging station with G2V and V2G charging configuration." *Journal of Green Engineering* 10.4 (2020).

[16].Priyadarshi, Neeraj, et al. "Performance evaluation of solar-PV-based non-isolated switched-inductor and switched-capacitor high-step-up cuk converter." *Electronics* 11.9 (2022): 1381.

[17]. Long, Wen, et al. "A novel grey wolf optimizer algorithm with refraction learning." *IEEE Access* 7 (2019): 57805-57819.

[18]. Mohamed, Ahmed AS, et al. "Grid integration of a PV system supporting an EV charging station using Salp Swarm Optimization." *Solar Energy* 205 (2020): 170-182.

[19]. Hao, Ying, et al. "Power forecasting-based coordination dispatch of PV power generation and electric vehicles charging in microgrid." *Renewable Energy* 155 (2020): 1191-1210.

[20]. Cao, Yan, et al. "An efficient terminal voltage control for PEMFC based on an improved version of whale optimization algorithm." *Energy Reports* 6 (2020): 530-542.

[21]. Mohamed, Ahmed AS, et al. "Grid integration of a PV system supporting an EV charging station using Salp Swarm Optimization." *Solar Energy* 205 (2020): 170-182.

[22]. Khan, Hussain Sarwar, et al. "Artificial neural network-based voltage control of DC/DC converter for DC microgrid applications." *2021 6th IEEE Workshop on the Electronic Grid (eGRID)*. IEEE, 2021.

[23]. Zhang, Dawei, Qing-Long Han, and Xian-Ming Zhang. "Network-based modeling and proportional–integral control for direct-drive-wheel systems in wireless network environments." *IEEE transactions on cybernetics* 50.6 (2019): 2462-2474.

[24]. Parvez, Mohammad, et al. "Comparative study of discrete PI and PR controls for single-phase UPS inverter." *IEEE Access* 8 (2020): 45584-45595.

[25]. Attia, Hussain A. "High performance PV system based on artificial neural network MPPT with PI controller for direct current water pump applications." *International Journal of Power Electronics and Drive Systems* 10.3 (2019): 1329-1338.

[26]. Maheswari Ellappan, Kavitha Anbukumar, Comparative Analysis of ACM and GPWM Controllers in Continuous Input and Output Power Boost PFC Converter, *Journal of Control Engineering and Applied Informatics*, Vol.22,No.4,2020.

[27] E.Maheswari, Dr.A.Kavitha (2016) Bifurcation analysis in continuous input output buck boost PFC converter, IEEE, ICCPEIC, 2016, 10.1109/ICCPEIC.2016.7557284.